

## Article

# Vulnerability Identification and Analysis of Contributors to Desertification in Inner Mongolia

Yang Chen <sup>1</sup>, Long Ma <sup>1,\*</sup>, Tingxi Liu <sup>1</sup>, Xing Huang <sup>1</sup> and Guohua Sun <sup>2</sup>

<sup>1</sup> College of Water Conservancy and Civil Engineering, Inner Mongolia Agricultural University, Hohhot 010018, China; chenyang@emails.imau.edu.cn (Y.C.)

<sup>2</sup> Bayannur City Hydrology and Water Resources Survey Center, Bayannur 015000, China

\* Correspondence: malong4444333@163.com

**Abstract:** Desertification vulnerability and contributing factors are of global concern. This study analyzed the spatial and temporal distribution of net primary productivity (NPP), precipitation, and temperature from 1985 to 2015. The rain use efficiency (RUE) of vegetation was selected as an indicator; and desertification vulnerability and contributors were evaluated with the Mann–Kendall test (M–K test) and the Thornthwaite–Memorial model. The results showed that NPP was lower in that years that had lower precipitation and higher temperatures, and vice versa. NPP was spatially consistent with precipitation distribution and roughly opposite to the spatial distribution of the annual change rate of temperature. The desertification vulnerability decreased from west to east, among which both the western sub–region (WSR) and the central sub–region (CSR) had the largest proportion of regions with high desertification vulnerability. On the other hand, the eastern sub–region (ESR) mostly comprises areas with extremely low or low desertification vulnerability. The vulnerability contributors for desertification differed among each sub–region. The desertified regions in WSR and ESR were mainly influenced by human activity (HA), but primarily driven by the combined impact of Precipitation–Temperature (PT) and HA in CSR. The south–east part of the CSR was only affected by HA, whereas the lesser affected regions in the study area were affected by PT and HA simultaneously. The study provides recommendations for the improvement of regional ecological environments to prevent future disasters.

**Keywords:** NPP; precipitation; temperature; desertification vulnerability; contributor; Inner Mongolia



**Citation:** Chen, Y.; Ma, L.; Liu, T.; Huang, X.; Sun, G. Vulnerability Identification and Analysis of Contributors to Desertification in Inner Mongolia. *Atmosphere* **2023**, *14*, 1170. <https://doi.org/10.3390/atmos14071170>

Academic Editors: Fanhao Meng, Min Luo and Wenfeng Chi

Received: 17 May 2023

Revised: 14 July 2023

Accepted: 16 July 2023

Published: 19 July 2023



**Copyright:** © 2023 by the authors. Licensee MDPI, Basel, Switzerland. This article is an open access article distributed under the terms and conditions of the Creative Commons Attribution (CC BY) license (<https://creativecommons.org/licenses/by/4.0/>).

## 1. Introduction

As one of the main types of land degradation [1], desertification is a hot spot in the field of global land degradation and restoration and has received extensive attention from international organizations such as the United Nations Convention to Combat Desertification [2]. Inner Mongolia is a typical representative of arid and semi–arid regions around the world and an important ecological barrier in northern China [3]. While desertification in this region is affected by both climate change and human activity, it can also respond quickly to changes in influencing factors. A qualitative or quantitative understanding of desertification vulnerability and its contributors is of great significance for curbing land degradation. However, Inner Mongolia has a vast territory and the differences in desertification vulnerability and desertification–causing factors in different sub–regions within the territory are not clear.

Currently, many scholars have conducted studies on the characteristics of desertification vulnerability and its contributors using the random forest model [4], Spearman rank correlation [5], and standard and adjusted Mediterranean desertification and land use approaches [6] with different time scales. The indicators used to measure desertification include the global desertification vulnerability index [7], the aridity index [8], the

normalized landscape index [9], and so on. The research scope covers the world [7], Central Asia [10], Iraq [11], Mongolia [12,13], and China [14,15], among others. The results showed that desertification has become one of the most severe ecological problems worldwide, affecting 20% of the world's population, 70% of the dry land, and 25% of global terrestrial land [16,17]. Among them, moderate desertification regions, severe desertification regions, and extremely severe desertification regions account for 13%, 7% and 9% of the world, respectively [7]. Desertification has occurred in varying degrees in most parts of Central Asia from the 1980s to the 2000s, and deteriorated further in the 2010s [10]. Climate change, drought or less rainfall, abuse of natural resources, overgrazing, and other factors were all found to be closely related to the aggravation of desertification in Iraq in the past two decades even posing a threat to food security and human health in the area [11]. Influenced by factors such as increased temperature and decreased precipitation, more than three-quarters of the land in Mongolia is being affected by drought and desertification [12]. Desertification in China is also grave: from 1950 to 2000, desertified regions in China increased from  $1.37 \times 10^5 \text{ km}^2$  to  $3.85 \times 10^5 \text{ km}^2$  [18] and the rate of desertification rose from  $1.56 \times 10^3 \text{ km}^2/\text{a}$  to  $3.60 \times 10^3 \text{ km}^2/\text{a}$  [19]. As of 2014, desertified regions in China accounted for 27.2% of the whole country, distributed across 18 provinces (municipalities and autonomous regions). Regions with mild desertification, moderate desertification, severe desertification, and extremely severe desertification accounted for 28.7%, 35.4%, 15.4% and 20.5% of the total, respectively [15]. Northwestern China has always been a region where desertification is more severe than in other regions. For example, the soil salinization of oases in Xinjiang and the desertification of land on the edge of oases are mainly attributed to human activity (such as poor management of land resources) [20]. Since the 1980s, desertification has become one of the major causes of the decline in the ecosystem in Inner Mongolia [21]. However, over the last two decades, the desertification area has been reduced by nearly 11% [22], and the net land restoration area during 2000–2010 and 2010–2020 was 35,800  $\text{km}^2$  and 65,300  $\text{km}^2$ , respectively [23].

Most of the existing related achievements have focused on the status of desertification in different regions [24]. However, the identification of desertification vulnerability is still scarce and a rational assessment system of desertification vulnerability has not been established. Most studies examined areas that were sensitive to climate change in arid and semi-arid regions as the study area for overall research [25], and there is little comparative analysis of commonalities and differences in the vulnerability and contributors of desertification in small-scale areas within a certain region. Based on the above, to ensure the research result is more representative and comprehensive, this article chose Inner Mongolia, which has a large expanse of territory and covers a large number of climate types, as the study area. Based on NPP, precipitation, and temperature raster datasets from 1985 to 2015, the commonalities and differences of desertification vulnerability and contributors in different local regions within Inner Mongolia were comprehensively compared and analyzed. The study not only provides an indication of how to improve the ecological environment but also enriches its actual achievement in this field.

## 2. Materials and Methods

### 2.1. Overview of the Study Area

The study area is the Inner Mongolia Autonomous Region ( $37^{\circ}24' \text{ N} \sim 53^{\circ}23' \text{ N}$ ,  $97^{\circ}12' \text{ E} \sim 126^{\circ}04' \text{ E}$ ) (Figure 1). Its total area is approximately  $118.3 \times 10^4 \text{ km}^2$ , with a stretch of 2400 km from east to west and 1700 km from north to south. The elevation ranges from  $-35 \text{ m}$  to 3499 m, accounting for 12.3% of China's total area. The Inner Mongolia Autonomous Region also has complex and varied landforms (e.g., deserts, mountains, plains, sand, and basins), with a variety of climate types (e.g., monsoon climate, temperate continental climate, and plateau climate) [26].

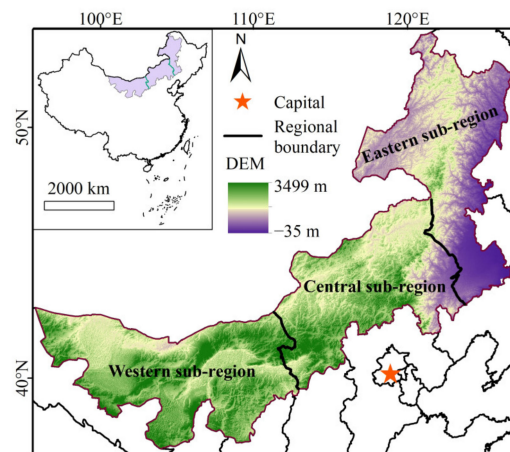


**Figure 1.** Location of the study area.

### 2.2. Materials

The precipitation and temperature data include monthly precipitation and temperature raster datasets with 1 km resolution in China, which were sourced from the national earth system science data center. The dataset was generated through a delta spatial downscaling scheme (mainly consisting of four steps: 1. Construction of the dataset. 2. Construction of the anomaly time series. 3. Spatial interpolation. 4. Conversion to absolute climatic time series) [27,28] based on the global climate dataset published by the Climatic Research Unit and the high-resolution climate dataset published by WorldClim. The NPP data used in this study are from a monthly NPP dataset covering China’s terrestrial ecosystems north of 18° N (1985~2015); the data were sourced from the Global Change Research Data Publishing & Repository [29]. The three datasets all ranged from January 1985 to December 2015. Based on monthly data, the sum of NPP and precipitation from January to December was defined as annual NPP and annual precipitation, respectively, and the mean temperature from January to December was defined as annual temperature.

### 2.3. Data Processing Method

ArcGIS software was adopted to convert and extract NPP, precipitation, and temperature data to obtain monthly data in the study area, and all data formats were unified in a tiff format.

As a land degradation process, desertification is essentially the decline of land productivity. RUE is the ratio of NPP to precipitation and synthesizes the variability of land production capacity at the regional scale to characterize the development of desertification. A decrease in RUE value indicates a decline in vegetation’s ability to convert water and nutrients into biomass, which increases desertification vulnerability in the study area [30]. RUE was applied to characterize the desertification vulnerability in the study area. The calculation formula for RUE is:

$$RUE = \frac{NPP}{P} \tag{1}$$

In the formula: P—annual precipitation.

The Thornthwaite–Memorial model was used to analyze contributors to desertification vulnerability [31,32]. The specific theoretical formulas of the model are:

$$PT_{RUE} = \frac{3000 \left[ 1 - e^{-0.0009695 \left[ \frac{1.05P}{\sqrt{1 + \left( \frac{1.05P}{3000 + 25T + 0.05T^3} \right)^2}} - 20 \right]} \right]}{P} \tag{2}$$

$$HA_{RUE} = PT_{RUE} - RUE \tag{3}$$

In the formula: T—annual temperature; P—annual precipitation;  $PT_{RUE}$ —desertification vulnerability related to PT ( $gC \cdot mm^{-1} \cdot m^{-2} \cdot a^{-1}$ );  $HA_{RUE}$ —desertification vulnerability related to HA ( $gC \cdot mm^{-1} \cdot m^{-2} \cdot a^{-1}$ ).

Based on the least squares method, the one-variable linear regression model was used to simulate the annual change rate of factors (including NPP, precipitation, temperature, RUE,  $PT_{RUE}$  and  $HA_{RUE}$ ) in the study area on the basis of each pixel [33]. The formula is:

$$\theta = \frac{n \sum_{i=1}^n i c_i - \sum_{i=1}^n i \sum_{i=1}^n c_i}{n \sum_{i=1}^n i^2 - (\sum_{i=1}^n i)^2} \tag{4}$$

In the formula:  $\theta$ —the annual change rate of factors ( $\theta_{NPP}$ ,  $\theta_P$ ,  $\theta_T$ ,  $\theta_{RUE}$ ,  $\theta_{PT_{RUE}}$  and  $\theta_{HA_{RUE}}$  were used to indicate the annual change rate of NPP, precipitation, temperature, RUE,  $PT_{RUE}$ , and  $HA_{RUE}$ , respectively, in the following paper);  $c_i$ —annual value of factors in the year  $i$ ;  $n$ —number of years in the calculation period.

The M-K test is a non-parametric test widely used in hydro-meteorological data analyses. Here, the M-K test was used to measure the significance of the annual change rate in factors [34]. The specific formulas are:

$$\text{sgn}(X_{k+1} - X_k) = \begin{cases} +1 & \text{if } X_{k+1} - X_k > 0 \\ 0 & \text{if } X_{k+1} - X_k = 0 \\ -1 & \text{if } X_{k+1} - X_k < 0 \end{cases} \tag{5}$$

$$S = \sum_{k=1}^{n-1} \sum_{k+1}^n \text{sgn}(X_{k+1} - X_k) \tag{6}$$

$$V(S) = \frac{n(n-1)(2n+5)}{18} \tag{7}$$

$$Z = \begin{cases} \frac{S-1}{\sqrt{V(S)}} & \text{if } S > 0 \\ 0 & \text{if } S = 0 \\ \frac{S+1}{\sqrt{V(S)}} & \text{if } S < 0 \end{cases} \tag{8}$$

In the formula:  $X_{k+1}$  and  $X_k$ —the value of factors in year  $k + 1$  and  $k$ ;  $S$ —the Kendall statistic;  $n$ —the length of data;  $V(S)$  —the variance of  $S$ ;  $Z$  —the test statistics. In addition, when  $|Z|$  is above or equal to 1.64, 1.92, and 2.32, it indicates that the annual change rate of factors passed significance tests at 90%, 95%, and 99% confidence levels.

#### 2.4. Criteria for Classification of Desertification Vulnerability and Identification of Contributors

The study defined the region with  $\theta_{RUE}$  above 0 and passed the M-K test with 95% confidence as the improved region and, based on whether  $\theta_{RUE}$  passed the test of significance with a confidence interval of 99%, the improved regions were further divided into the region with moderate improvement and the region with significant improvement. See Table 1 for details.

With reference to previous research results [30], the study divided the positive and negative combinations of  $\theta_{RUE}$ ,  $\theta_{PT_{RUE}}$  and  $\theta_{HA_{RUE}}$  into 8 scenarios (Table 2) to measure the driving effects of PT or HA on improved regions and desertified regions. If  $\theta_{PT_{RUE}}$  was positive or  $\theta_{HA_{RUE}}$  was negative, it meant that either PT or HA helped in the recovery of desertification. If  $\theta_{PT_{RUE}}$  was negative or  $\theta_{HA_{RUE}}$  was positive, it indicated that either PT or HA aggravated desertification.

**Table 1.** Criteria for desertification vulnerability classification.

Regions	Z Value	Classification
Improved regions	$2.32 \leq Z$	Region with significant improvement
	$1.96 \leq Z < 2.32$	Region with moderate improvement
Desertified regions	$0 \leq Z < 1.96$	Region with extremely low desertification vulnerability
	$-1.96 \leq Z < 0$	Region with low desertification vulnerability
	$-2.32 \leq Z < -1.96$	Region with moderate desertification vulnerability
	$Z < -2.32$	Region with high desertification vulnerability

**Table 2.** Quantitative assessment models of PT and HA.

Regions	$\theta_{PT_{RUE}}$	$\theta_{HA_{RUE}}$	Contributor
Improved regions	$>0$	$>0$	PT
	$>0$	$<0$	Both
	$<0$	$>0$	Error
	$<0$	$<0$	HA
Desertified regions	$>0$	$>0$	HA
	$>0$	$<0$	Error
	$<0$	$>0$	Both
	$<0$	$<0$	PT

In addition, when the desertified region (improved region) was affected by PT and HA at the same time, this study calculated the contribution rate of the two using the following formula:

$$C_{PT_{RUE}(HA_{RUE})} = \frac{|\theta_{PT_{RUE}(HA_{RUE})}|}{|\theta_{PT_{RUE}}| + |\theta_{HA_{RUE}}|} \times 100\% \tag{9}$$

In the formula: C—contribution rate of PT or HA.

In summary, the identification and attribution of desertification vulnerability were mainly divided into two steps (Figure 2): 1. Identification of desertification vulnerability. 2. Determination and quantitative analysis of contributors to desertification vulnerability.

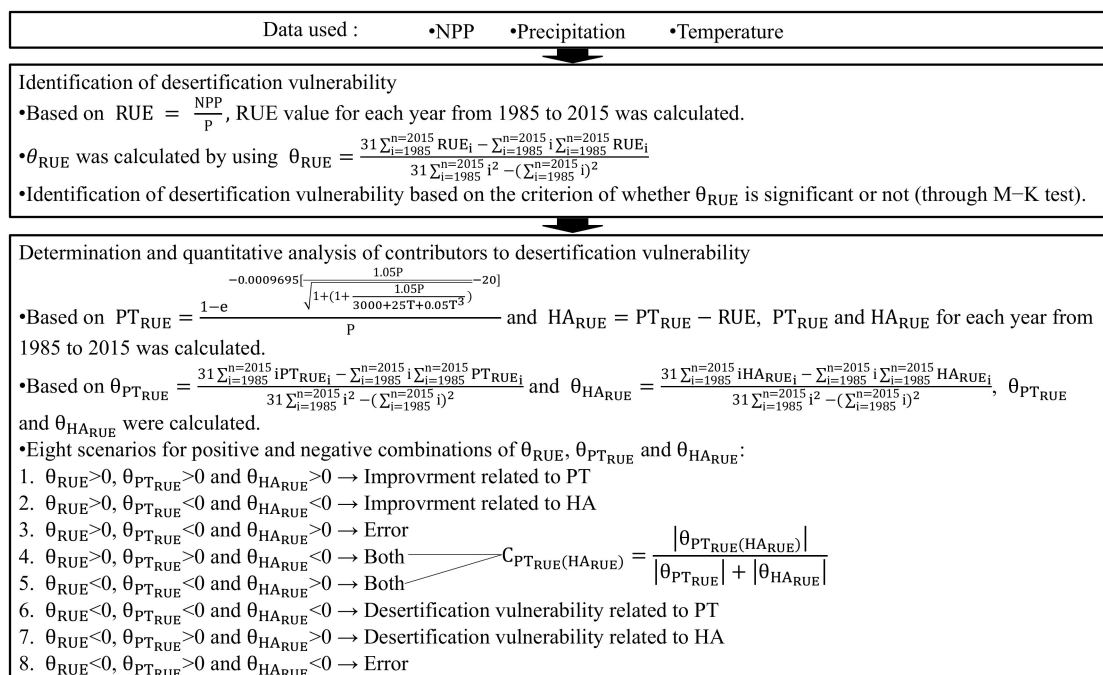


**Figure 2.** The process of identification and attribution of desertification vulnerability.

### 2.5. Division of the Study Area

The study area was large, with significant differences in NPP, precipitation, and temperature from west to east (as shown in Figure 3a,b). To facilitate analysis, it was rationalized based on the administrative boundaries as well as the practice of previous regional divisions [26]. The study area was divided into three sub-regions (Figure 3c): the western sub-region (including Alxa League, Wuhai, Bayannur, Baotou, and Ordos); the central sub-region (Hohhot, Ulanqab, Chifeng, and Xilin Gol League); and the eastern sub-region (Tongliao, Hulunbeier, and Xing'an League).

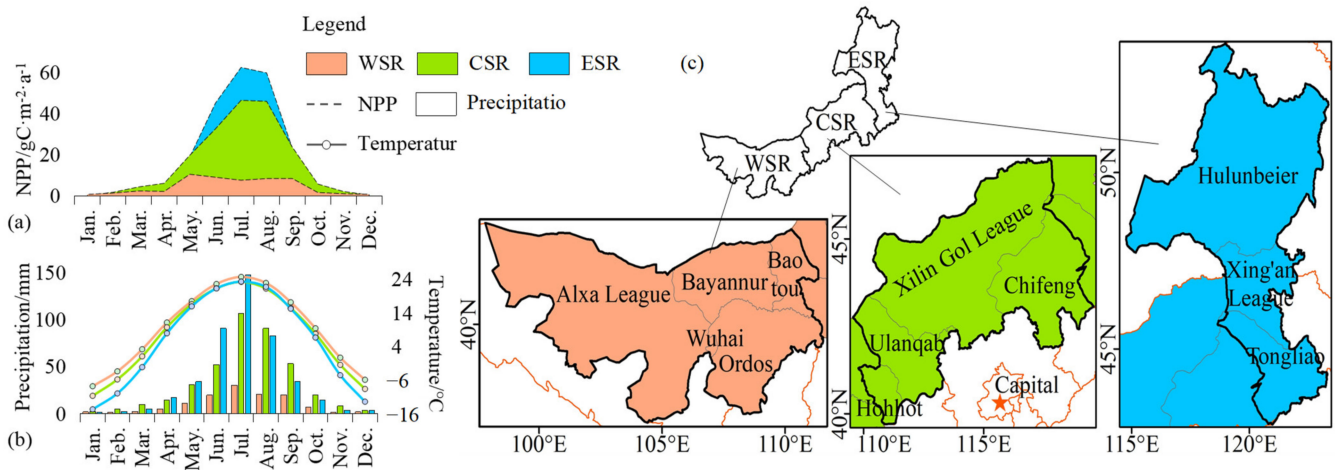


**Figure 3.** (a) The regional mean value of NPP for WSR, CSR, and ESR. (b) The regional mean value of precipitation and temperature for WSR, CSR, and ESR. (c) Regionalization of WSR, CSR, and ESR.

## 3. Results

### 3.1. Spatio-Temporal Changes of NPP, Precipitation, and Temperature

Figure 4 shows the spatio-temporal variation of NPP and spatial distribution of  $\theta_{NPP}$  in the study area. It can be seen from the figure that the regional mean values of NPP in WSR, CSR, and ESR from 1985 to 2015 were  $100.94 gC \cdot m^{-2} \cdot a^{-1}$ ,  $171.66 gC \cdot m^{-2} \cdot a^{-1}$ , and  $233.06 gC \cdot m^{-2} \cdot a^{-1}$ , respectively. The maximum value (minimum value) appeared in 1998 (2005), 1998 (2007), and 2014 (1992). In terms of the temporal evolution of the NPP, the NPP values of WSR and CSR were relatively high from 1985 to 1999 and decreased rapidly after entering the 21st century; while the NPP value in ESR fluctuated with an upward trend on the whole. In spatial terms, the annual average NPP of WSR and CSR was lower in the west, higher in the east, and the dividing line was roughly at  $109.5^{\circ} E$  and  $118^{\circ} E$ . The annual NPP of ESR was higher in Great Khingan and its surrounding areas and gradually decreased toward the south and the west.

The annual change rate of NPP in WSR mainly decreased (accounting for approximately 74.25% of the total area of WSR). An amount of 68.57% of the decreased region passed the test of significance, which was mainly distributed in the east of the Badain Jaran Desert. The rate of decline was between  $-23.55 \sim -2.00 gC \cdot m^{-2} \cdot a^{-1} / 10 a$ . On the other hand, 25.75% of WSR showed an upward trend, and the area which passed the significance test accounted for 20.62%. In spatial terms, the NPP increased at a faster rate in the south and the north but at a slower rate in the central part. The annual change rate of NPP in CSR increased on the whole, accounting for 53.15% of CSR, with 41.05% of CSR seeing a significant increase, mostly at the rate of  $10 gC \cdot m^{-2} \cdot a^{-1} / 10 a$  or more. Regions with a decreasing annual change rate of NPP were mainly concentrated in northern Ulanqab and western Xilinhot (part of the Xilin Gol League). The area that passed the test of significance with a confidence level of 95% accounted for 35.11%, and the rate of decline exceeded  $-13.45 gC \cdot m^{-2} \cdot a^{-1} / 10 a$ . The  $\theta_{NPP}$  in ESR was between  $-23.82 gC \cdot m^{-2} \cdot a^{-1} / 10 a$  and  $17.37 gC \cdot m^{-2} \cdot a^{-1} / 10 a$ ; the overall distribution was that NPP decreased (36.89%) in the central part and increased (63.11%) in the north-south. Among them, the areas that decreased

significantly and increased significantly accounted for 22.20% and 44.35%, respectively. The NPP increased region was mainly distributed near Hulun Lake, while the NPP decreased region was concentrated in the south of ESR.

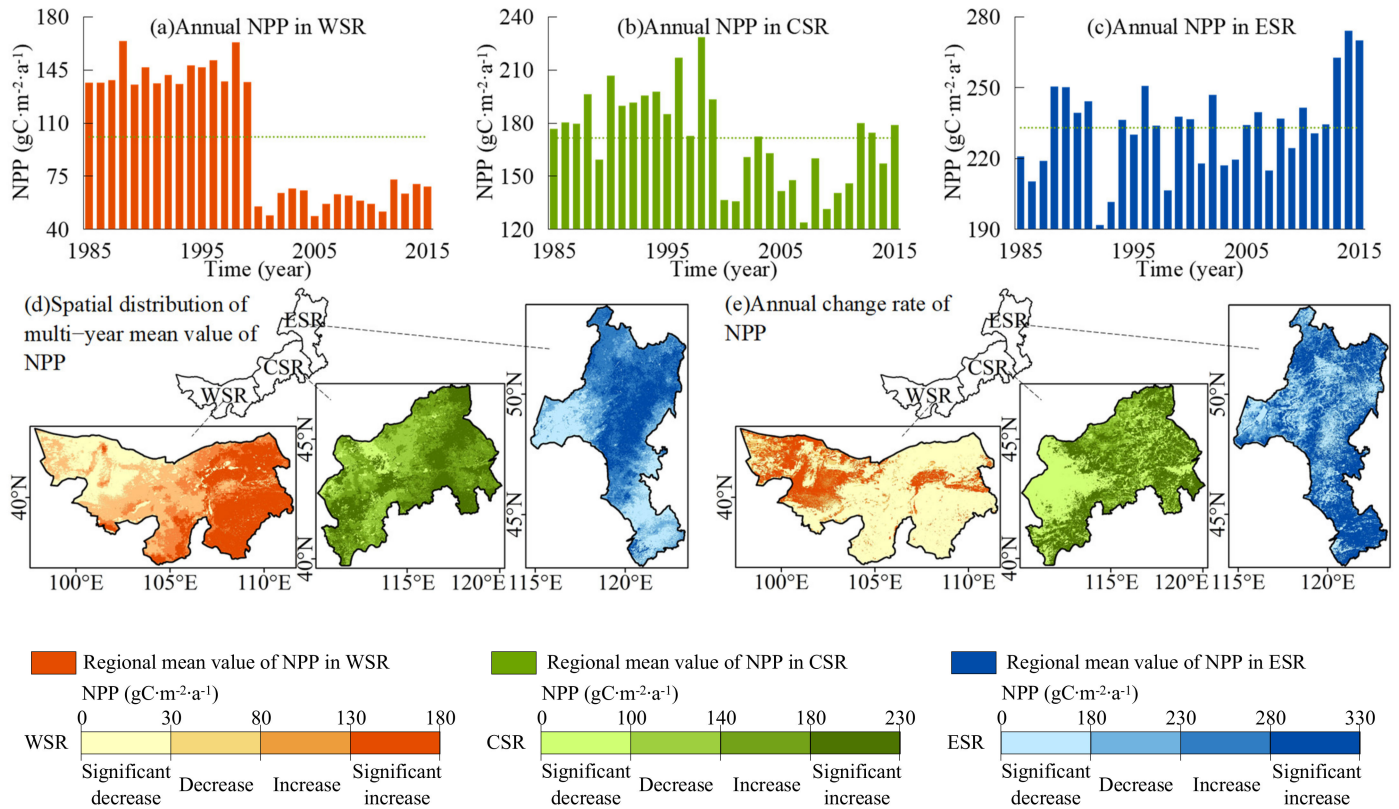


**Figure 4.** (a) The regional mean value of NPP for WSR. (b) The regional mean value of NPP for CSR. (c) The regional mean value of NPP for ESR. (d) Spatial distribution of NPP’s multi-year mean value in different sub-regions. (e) Spatial distribution of NPP’s annual change rate in different sub-regions.

Figure 5 shows the spatio-temporal variation of precipitation and the spatial distribution of  $\theta_p$  in the study area. The annual precipitation of WSR, CSR, and ESR was 289.67 mm, 292.52 mm, and 425.19 mm, respectively. All the maximum values appeared in 1998, and the minimum values appeared between 2005 and 2007. The spatio-temporal changes of precipitation in the three sub-regions have remarkable consistency: showing a rising trend first, then falling and rising again temporally, and rising from west to east (from northwest to southeast) spatially.

In terms of the annual change rate of precipitation in the three sub-regions, except for the junction of WSR and CSR as well as the surrounding areas of Mu Us Sandland, the annual precipitation of WSR was mainly on the rise, accounting for 89.99% of WSR, yet the rate of rise was very slow ( $\theta_p$  was mostly between 0~7 mm/a). Only about 5.61% of the area increased significantly, and the rate was above 7.5 mm/a. The annual precipitation of CSR and ESR dropped, and the rate of decrease rose from west to east and from north to south. Among them, 42.08% of CSR had a significant decreasing trend in annual precipitation, which was mainly concentrated in the regions east of 120° E, with the annual precipitation decreasing at a rate between 1.68 and 3.83 mm/a. A total of 11.82% of the ESR showed a significant downward trend, most of which were concentrated in Tongliao. The annual change rates of precipitation in the rest of CSR and ESR were between -2~0.31 mm/a and -2~0.34 mm/a, thus the change of precipitation in these areas was not significant.

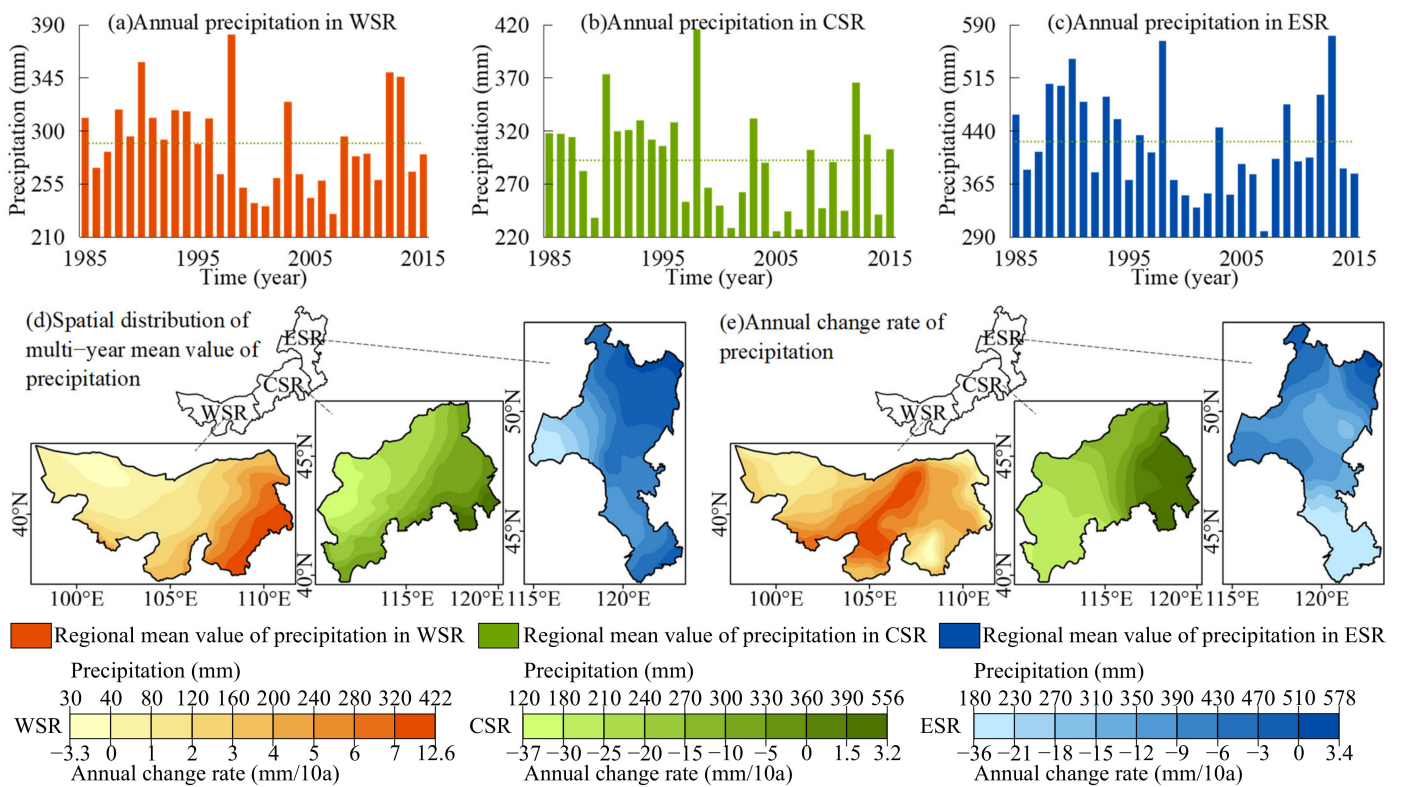


**Figure 5.** (a) The regional mean value of precipitation for WSR. (b) The regional mean value of precipitation for CSR. (c) The regional mean value of precipitation for ESR. (d) Spatial distribution of precipitation's multi-year mean value in different sub-regions. (e) Spatial distribution of precipitation's annual change rate in different sub-regions.

Figure 6 shows the spatio-temporal variation of temperature and the spatial distribution of  $\theta_T$  in the study area. The annual temperature in the study area decreased from west to east as a whole, and the regional average temperatures of WSR, CSR, and ESR were 7.91 °C, 3.64 °C, and 0.59 °C, respectively. The average temperature of the three sub-regions fluctuated temporally. Among them, the average temperature of CSR increased at the fastest rate (0.37 °C/10 a), followed by WSR and ESR (0.139 °C/10 a). The annual temperature of WSR and ESR increased from west to east and from north to south, respectively. As to CSR, the annual temperature of its center, Hunshandake Sandy Land was the lowest, and increased toward the southeast and the southwest.

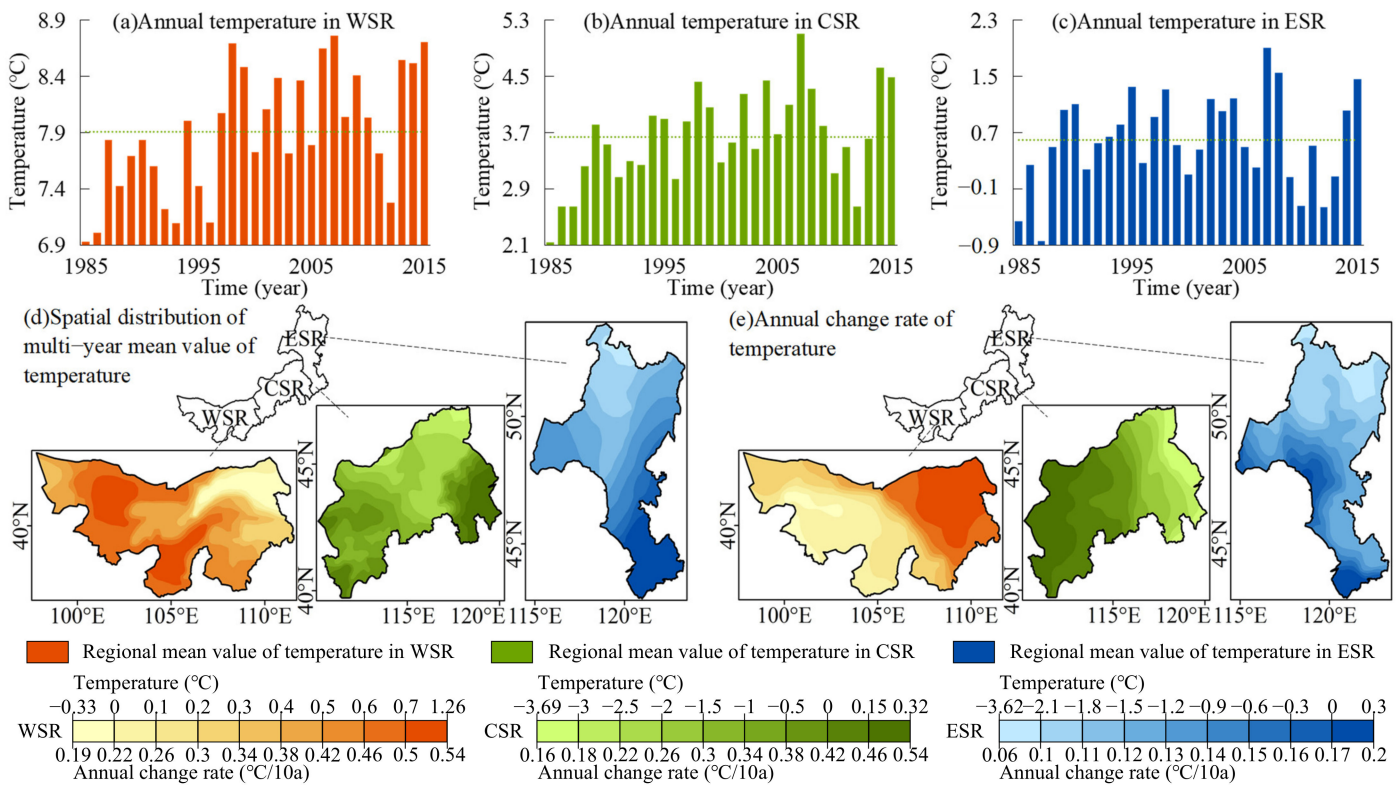
The annual change rate of temperature in both WSR and CSR increased significantly; the former increased at a faster rate from west to east, while that of the CSR increased at the same rate from east to west. The annual change rate of temperature in ESR also rose, yet the  $\theta_T$  was mostly less than 0.05 °C/10 a, which failed to pass the test of significance.

### 3.2. Spatio-Temporal Variation in Desertification Vulnerability and Its Contributors

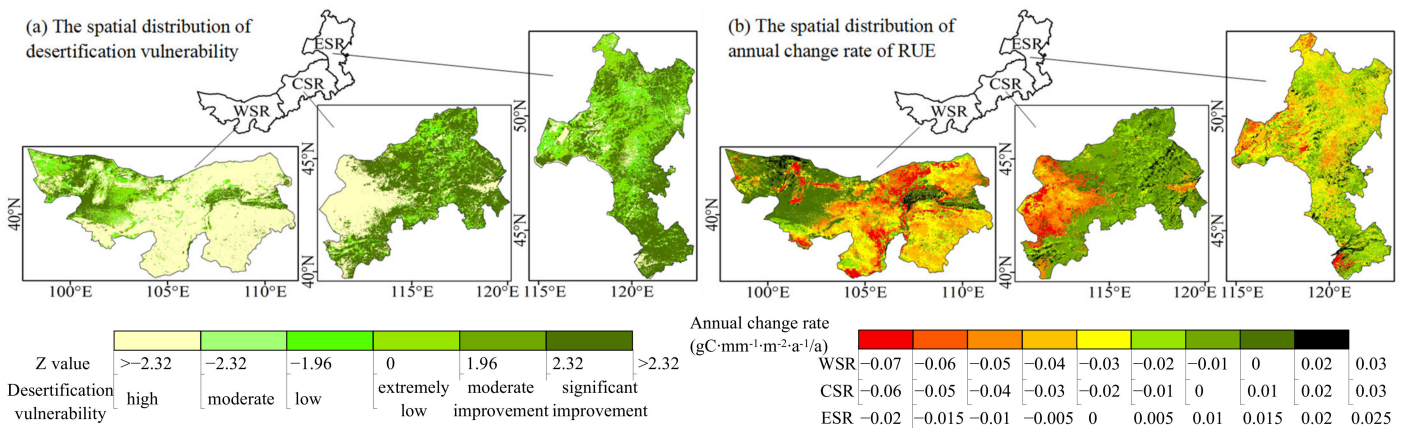
#### 3.2.1. Spatial and Temporal Distribution Characteristics of Desertification Vulnerability

Figure 7 shows the spatial distribution of desertification vulnerability (a) and the annual change rate of RUE in the study area from 1985 to 2018 (b). According to the figure, WSR was a desertified region as a whole, accounting for 84.41% of the total area, and 69.73% of WSR belonged to the regions with high or moderate desertification vulnerability, which were mainly distributed from the Jilantai Saline Land to the Urat Rear Banner (part of Bayannur). The  $\theta_{RUE}$  in this region was between  $-0.068 \text{ gC}\cdot\text{mm}^{-1}\cdot\text{m}^{-2}\cdot\text{a}^{-1}/\text{a}$  and  $-0.027 \text{ gC}\cdot\text{mm}^{-1}\cdot\text{m}^{-2}\cdot\text{a}^{-1}/\text{a}$ . Regions with low or extremely low desertification vulnerability accounted for 14.68% of the total area of WSR, mainly distributed in the west of Ejina Banner (part of Alxa League) and the northwest of Alxa Right Banner (part of Alxa League). The regions with moderate improvement and significant improvement accounted

for 1.93% and 13.66% of the total, mainly distributed in the central part of Ejina Banner (part of Alxa League), where the  $\theta_{RUE}$  was mostly above  $0.02 \text{ gC}\cdot\text{mm}^{-1}\cdot\text{m}^{-2}\cdot\text{a}^{-1}/\text{a}$ .



**Figure 6.** (a) The regional mean value of temperature for WSR. (b) The regional mean value of temperature for CSR. (c) The regional mean value of temperature for ESR. (d) Spatial distribution of temperature’s multi-year mean value in different sub-regions. (e) Spatial distribution of temperature’s annual change rate in different sub-regions.



**Figure 7.** (a) Spatial distribution of desertification vulnerability in each sub-region. (b) Spatial distribution of RUE’s annual change rate in different sub-regions.

The overall desertification vulnerability level of CSR was relatively simple and had prominent spatial differences. Specifically, desertified regions and improved regions accounted for 47.38% and 52.62% of total CSR, respectively. Among them, desertified regions were mainly concentrated in the northwest of CSR, including Darhan Muminggan United Banner (part of Baotou), Siziwang Banner (part of Ulanqal), and other places. Most were desertified regions with high desertification vulnerability (regions with moderate, low,

and extremely low desertification vulnerability accounted for only 0.76%, 6.02%, and 9.61% of CSR, respectively), and the  $\theta_{RUE}$  was between  $-0.055 \text{ gC}\cdot\text{mm}^{-1}\cdot\text{m}^{-2}\cdot\text{a}^{-1}/\text{a}$  and  $-0.026 \text{ gC}\cdot\text{mm}^{-1}\cdot\text{m}^{-2}\cdot\text{a}^{-1}/\text{a}$  in this area. The region with moderate improvement only accounted for 2.36% of the CSR, and the remainder were all regions with significant improvement (50.26%), where the RUE mostly grew by  $0.005 \text{ gC}\cdot\text{mm}^{-1}\cdot\text{m}^{-2}\cdot\text{a}^{-1}/\text{a}$  to  $0.02 \text{ gC}\cdot\text{mm}^{-1}\cdot\text{m}^{-2}\cdot\text{a}^{-1}/\text{a}$ , and in spatial terms, the RUE rose at the fastest rate in the east of the CSR and gradually decreased in the west.

From north to south, the ESR was characterized by a sandwich structure of “improved regions–desertified regions–improved regions”, accounting for 50.46% and 49.54% of the ESR, respectively. Among them, the area with significantly improved RUE accounted for 44.41% of ESR, and the  $\theta_{RUE}$  in this region was mostly above  $0.005 \text{ gC}\cdot\text{mm}^{-1}\cdot\text{m}^{-2}\cdot\text{a}^{-1}/\text{a}$ . Desertified regions were mainly distributed in the central part of ESR, of which the regions with extremely low, low, moderate, and high desertification vulnerability accounted for 23.83%, 14.27%, 1.64%, and 10.72% of ESR, respectively. In space, the desertified regions with moderate and high desertification vulnerability were mainly concentrated near Hulun Lake, and the vulnerability level decreased eastward.

### 3.2.2. Determination and Quantitative Analysis of Contributors to Desertification Vulnerability

Figure 8 shows the spatial distribution of contributors to desertification vulnerability in the study area. As mentioned above, 84.41% belonged to desertified regions, of which 61.96% of the WSR was caused by HA, 0.74% was caused by PT (which was mainly concentrated at the junction of WSR and CSR), and 16.55% of the area was affected by a combination of PT and HA; the contribution rates of the two were 53.6% ( $\theta_{PT_{RUE}} = -1.19 \times 10^{-3} \text{ gC}\cdot\text{mm}^{-1}\cdot\text{m}^{-2}\cdot\text{a}^{-1}/\text{a}$ ) and 46.4% ( $\theta_{HA_{RUE}} = 1.03 \times 10^{-3} \text{ gC}\cdot\text{mm}^{-1}\cdot\text{m}^{-2}\cdot\text{a}^{-1}/\text{a}$ ), respectively. The improved regions accounted for 15.59% of WSR. and the joint effect of PT and HA was the leading factor for the improvement of desertification in this region (12.18%). The contribution rates of the two factors in the improved regions were 28.64% ( $\theta_{PT_{RUE}} = 3.11 \times 10^{-3} \text{ gC}\cdot\text{mm}^{-1}\cdot\text{m}^{-2}\cdot\text{a}^{-1}/\text{a}$ ) and 71.36% ( $\theta_{HA_{RUE}} = -3.11 \times 10^{-3} \text{ gC}\cdot\text{mm}^{-1}\cdot\text{m}^{-2}\cdot\text{a}^{-1}/\text{a}$ ), respectively, followed by HA (1.79%), while the area which had improved under the influence of PT only accounted for 1.45% of WSR.

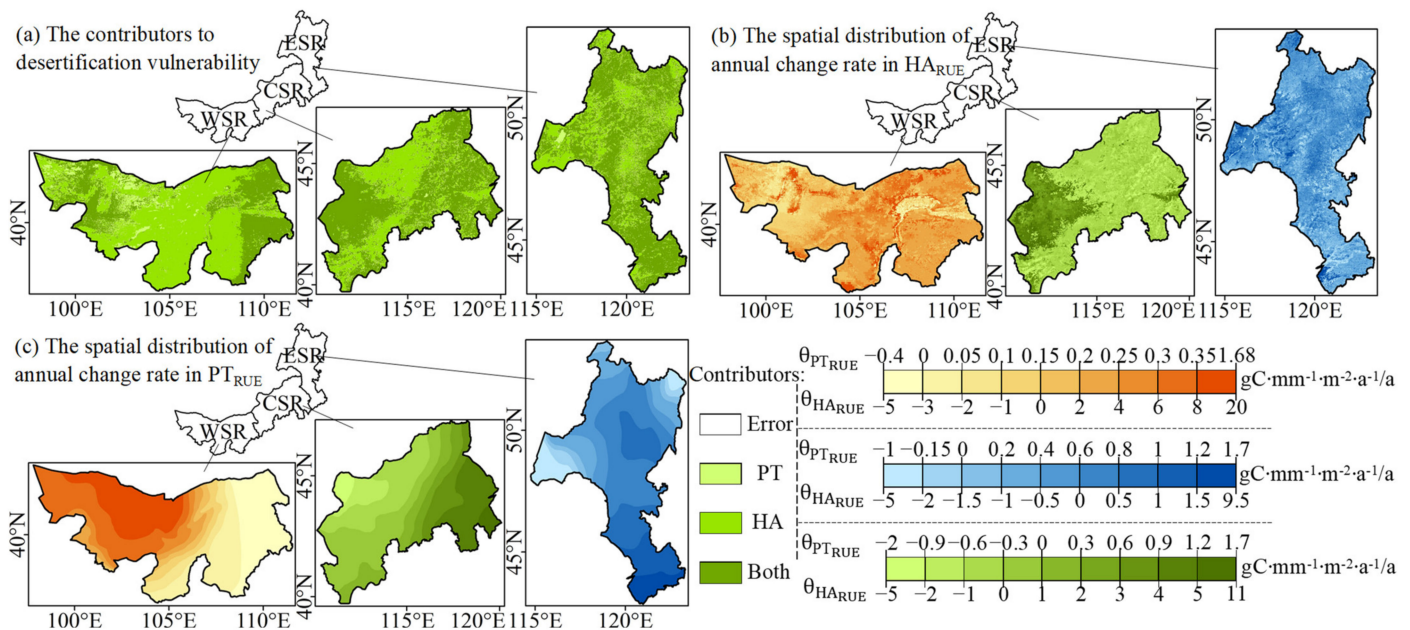


**Figure 8.** (a) Spatial distribution of contributors to desertification vulnerability in different sub-regions. (b) Spatial distribution of  $HA_{RUE}$ 's annual change rate in different sub-regions. (c) Spatial distribution of  $PT_{RUE}$ 's annual change rate in different sub-regions.

Desertified regions and improved regions accounted for 47.38% and 52.62% of CSR, respectively. Of these, 20.83% were improved under the influence of HA and approximately 29.68% were improved under the joint influence of PT and HA; among them, the contribution rate of PT only accounted for 9.07%. In addition, the improved area that was only affected by PT accounted for 1.25%. Desertified regions were mostly caused by the joint effects of PT and HA (accounting for 26.46% of CSR), of which the contribution rate of PT was roughly 2.88% ( $\theta_{PT_{RUE}} = -0.41 \times 10^{-3} \text{ gC}\cdot\text{mm}^{-1}\cdot\text{m}^{-2}\cdot\text{a}^{-1}/\text{a}$ ), and the rest stemmed from HA. In addition, 9.35% and 5.73% of the desertified regions were derived from HA and PT, respectively.

The regions affected by both PT and HA accounted for 47.26% of ESR; the contribution rates of PT and HA were 19.71% ( $\theta_{PT_{RUE}} = 1.47 \times 10^{-3} \text{ gC}\cdot\text{mm}^{-1}\cdot\text{m}^{-2}\cdot\text{a}^{-1}/\text{a}$ ) and 82.29% ( $\theta_{HA_{RUE}} = -6.00 \times 10^{-3} \text{ gC}\cdot\text{mm}^{-1}\cdot\text{m}^{-2}\cdot\text{a}^{-1}/\text{a}$ ), respectively, most of which were improved regions. The desertified region in ESR was an area greatly affected by HA as 25.02% of ESR deteriorated under the influence of HA alone. Regions which were independently affected by PT were less than 5%.

#### 4. Discussion and Conclusions

The NPP in the study area was positively correlated with precipitation [35] and negatively correlated with temperature (Table 3). This is consistent with the correlation between NPP and precipitation or temperature in the Shendong coal mine [36], The overall correlation decreased from west to east (WSR > CSR > ESR). Such correlation is also demonstrated as follows: the NPP of WSR and CSR in years with less precipitation and higher temperature was lower, and vice versa. This further explains that precipitation and temperature may be important contributors to the NPP of WSR and CSR [37], and the NPP can also respond significantly to changes in precipitation and temperature. Zhang et al. proposed [38] that decreased precipitation, increased temperature, and potential evapotranspiration causes severe water deficiency and reduced ecosystem productivity, which is consistent to some degree with this study. However, the NPP of ESR did not show such a correlation with precipitation and temperature, which may stem from factors such as suitable hydrothermal conditions and the good vegetation foundation of ESR. The overall NPP in the study area increased from west to east, that is, the regional mean value of the NPP of WSR was less than that of CSR as well as ESR, which is basically consistent with the spatial distribution of precipitation in the study area, and opposite to the temperature to a certain degree. From the perspective of the annual change rate, the NPP in WSR mostly dropped, while that in CSR and ESR rose. On the whole, NPP decreased more rapidly in regions where temperature rose at a faster rate, and tended to increase in regions where temperature rose at a slower rate. The conclusion that the change of NPP in the Hunshandake Sandy Land is closely linked to the change of precipitation and temperature is basically consistent with this article [39]. However, since 2000, NDVI has been weakly related to precipitation [40] and other studies have different conclusions to the results of this study, which may be due to the difference in the selection of the index.

**Table 3.** Correlation between NPP and precipitation or temperature.

WSR		CSR		ESR	
Precipitation	Temperature	Precipitation	Temperature	Precipitation	Temperature
0.49 *	−0.45 *	0.80 *	−0.23	0.11	0.06

Note: "\*" in the table referred to significantly correlated at the 0.05 level.

As shown in Figure 9, the overall desertification vulnerability in the study area decreased from west to east. Among them, both WSR and CSR had the largest proportion of regions with high vulnerability to desertification, followed by low desertification vulnerability regions, extremely low desertification vulnerability regions, and moderate desertification vulnerability regions. On the other hand, ESR consisted mostly of regions with

extremely low desertification vulnerability, followed by low desertification vulnerability, high desertification vulnerability, and moderate desertification vulnerability regions. The proportion of improved regions decreased from the central part to the east and west as a whole. To be more precise, the improved regions in CSR were larger than those in WSR and ESR, and the area of improved regions in CSR was 2~3 times larger than that in WSR and ESR.

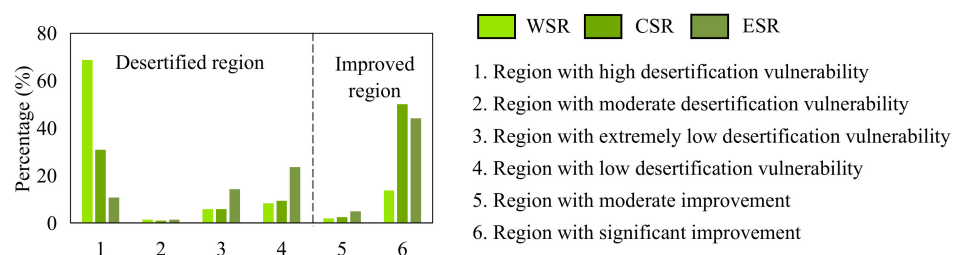


**Figure 9.** The proportion of areas with different desertification vulnerability in each sub-region.

As a whole, the combined effort of PT and HA contributed significantly to desertification vulnerability in the study area. However, there were some regional differences as well. For example, PT and HA were both key contributors to CSR's desertification vulnerability in desertified regions, while in WSR and ESR, desertified regions were mainly influenced by HA alone. Improved regions in the study area were primarily driven by both, but the improved region in the southeast part of the CSR was only dependent on HA. The conclusion is that there are temporal and spatial differences in the impact of climate change, natural variability, and HA on desertification. For example, changes in climate factors were the main reason for the fluctuation of desertification boundaries in arid and extremely arid regions of Inner Mongolia [31] and there were no obvious signs of desertification expansion in the Hunshandake Sandy Land under climate change and HA [39]. Grassland desertification is becoming increasingly serious, and human activity is a major factor in the occurrence of desertification in an increasing number of areas [5]. These are all consistent with this article to a certain extent. However, the conclusion that the improvement of desertification in the China–Mongolia–Russia Economic Corridor was dominated by climate change [41] and desertification was the result of the superposition of climate and HA, with climate change being the main influencing factor followed by HA [42] differs from the results of this study, which may be due to the difference in the study area and study period.

This article provides a detailed analysis of desertification vulnerability and its contributors in Inner Mongolia. However, the article also has certain gaps in its methods. For example,  $HA_{RUE}$  cannot be defined by  $RUE$  and  $PT_{RUE}$  entirely; if heavy rains have brought fertile soil from upstream downstream, the corresponding portion of biomass would also be included in the  $HA_{RUE}$ , even if it is not of anthropogenic origin. Conversely, in the presence of a parasitic attack (which reduces NPP), the effective  $HA_{RUE}$  linked to anthropogenic effects would be biased (reduced). Based on the annual change rate of  $RUE$ ,  $PT_{RUE}$ , and  $HA_{RUE}$ , the driving effects of PT and HA on desertification vulnerability were divided into eight scenarios for discussion, but whether there is a more logical way to divide the scenarios needs to be explored further. Studies have shown that wind [43], overgrazing, deforestation [44], and overcultivation [45] are also important contributors to desertification. Anthropogenic activity is a double-edged sword for vegetation change [46]. Thus, based on multiple factors and methods, an in-depth analysis of the relationship between these factors and desertification should be conducted.

**Author Contributions:** Conceptualization, Y.C. and L.M.; methodology, L.M.; software, Y.C.; validation, Y.C., L.M. and G.S.; formal analysis, L.M.; investigation, T.L.; resources, L.M.; data curation, Y.C.; writing—original draft preparation, Y.C.; writing—review and editing, Y.C.; visualization, X.H.; supervision, X.H.; project administration, L.M.; funding acquisition, L.M. All authors have read and agreed to the published version of the manuscript.

**Funding:** This research was funded by the Technology–Planning Project of Inner Mongolia (2020GG0074) and the Inner Mongolia Science Foundation (2020MS05054).

**Institutional Review Board Statement:** Not applicable.

**Data Availability Statement:** The precipitation and temperature data used were from the national earth system science data center (<http://www.geodata.cn/>) (accessed on 7 April 2023), and provided by the team of Professor Shouzhang Peng of Northwest A&F University, China. The NPP data used was accessed from the global change research data publishing repository (<https://www.geodoi.ac.cn/WebCn>) (accessed on 7 April 2023), provided by Professor Pengfei Chen from the University of Chinese Academy of Sciences, China.

**Conflicts of Interest:** The authors declare no conflict of interest.

## References

1. Ci, L.J. Understanding on the term of “Desertification”. *Chin. Sci. Technol. Terms J.* **2000**, *2*, 11–13.
2. UNCCD. *United Nations Convention to Combat Desertification in Countries Experiencing Serious Drought and/or Desertification, Particularly in Africa*; Secretariat of the United Nations Convention to Combat Desertification: Bonn, Germany, 1994.
3. Wei, Y.J.; Zhu, L.; Chen, Y.; Cao, X.Y.; Yu, H.L. Spatiotemporal Variations in Drought and Vegetation Response in Inner Mongolia from 1982 to 2019. *Remote Sens.* **2022**, *14*, 3803. [[CrossRef](#)]
4. Dharumarajan, S.; Bishop, T.F.A. Desertification status mapping in Muttuma Watershed by using Random Forest Model. *Sci. Cold Arid. Reg.* **2022**, *14*, 32–42.
5. Yi, Y.; Shi, M.C.; Yang, N.; Zhang, C.; Yi, X.D. Spatio-Temporal Patterns and Driving Forces of Desertification in Otindag Sandy Land, Inner Mongolia, China, in Recent 30 Years. *Remote Sens.* **2023**, *15*, 279. [[CrossRef](#)]
6. Jinan, A.A.A. Assessment of land sensitivity to desertification for Al Mussaib project using MEDALUS approach. *Casp. J. Environ. Sci.* **2022**, *20*, 177–196.
7. Huang, J.P.; Zhang, G.L.; Zhang, Y.T.; Guan, X.D.; Wei, Y.; Guo, R.X. Global desertification vulnerability to climate change and human activities. *Land Degrad. Dev.* **2020**, *31*, 1380–1391. [[CrossRef](#)]
8. Jessica, B.D.M.; Henderson, S.W.; Rafael, C.D. Areas susceptible to desertification in Brazil and projected climate change scenarios. *Nat. Hazards* **2023**, *116*, 1463–1483.
9. Yu, X.W.; Zhuo, Y.; Liu, H.M.; Wang, Q.; Wen, L.; Li, Z.Y.; Liang, C.Z.; Wang, L.X. Degree of desertification based on normalized landscape index of sandy lands in inner Mongolia, China. *Glob. Ecol. Conserv.* **2020**, *23*, e01132. [[CrossRef](#)]
10. Cai, D.W.; Wang, X.M.; Hua, T.; Jiao, L.L.; Geng, X. Baseline and status of desertification in Central Asia. *Land Degrad. Dev.* **2022**, *33*, 771–784. [[CrossRef](#)]
11. Zuhair, F.A.F. Desertification in Iraq and how to Combatit. *IOP Conf. Ser. Earth Environ. Sci.* **2020**, *553*, 012033.
12. Han, J.; Dai, H.; Gu, Z.L. Sandstorms and desertification in Mongolia, an example of future climate events: A review. *Environ. Chem. Lett.* **2021**, *19*, 4063–4073. [[CrossRef](#)] [[PubMed](#)]
13. Liang, X.Y.; Li, P.F.; Wang, J.L.; Chan, F.K.S.; Togtokh, C.; Ochir, A.; Davaasuren, D. Research Progress of Desertification and Its Prevention in Mongolia. *Sustainability* **2021**, *13*, 6861. [[CrossRef](#)]
14. Li, C.L.; Wang, Y.; Gao, Z.H.; Sun, B. Spatial and temporal characteristics of forest and grass cover in the potential range of desertification in China from 2000 to 2020. *Acta Geogr. Sin.* **2022**, *77*, 2803–2816.
15. Tu, Z.F.; Li, M.X.; Sun, T. The Status and Trend Analysis of Desertification and Sandification. *For. Resour. Manag.* **2016**, *1*, 1–5.
16. Binal, A.C.; Dhinwa, P.S.; Ajai. Long term monitoring and assessment of desertification processes using medium & high resolution satellite data. *Appl. Geogr.* **2018**, *97*, 10–24.
17. D’Odorico, P.; Bhattachan, A.; Davis, K.F.; Ravi, S.; Runyan, C.W. Global desertification: Drivers and feedbacks. *Adv. Water Resour.* **2013**, *51*, 326–344. [[CrossRef](#)]
18. Wang, T.; Yan, C.Z.; Song, X.; Xie, J.L. Monitoring recent trends in the area of aeolian desertified land using Landsat images in China’s Xinjiang region. *ISPRS J. Photogramm. Remote Sens.* **2012**, *68*, 184–190. [[CrossRef](#)]
19. Wang, T.; Xue, X.; Zhou, L.; Guo, J. Combating aeolian desertification in northern China. *Land Degrad. Dev.* **2015**, *26*, 118–132. [[CrossRef](#)]
20. Yu, X.; Lei, J.Q.; Gao, X. An over review of desertification in Xinjiang Northwest China. *J. Arid. Land* **2022**, *14*, 1181–1195. [[CrossRef](#)]
21. Xu, D.Y. The Impact of Desertification Dynamics on Regional Ecosystem Services: A Case Study of Inner Mongolia (China). In *Community and Global Ecology of Deserts*; IntechOpen: London, UK, 2018. [[CrossRef](#)]

22. Guo, X.N.; Chen, R.S.; Thomas, D.S.G.; Li, Q.; Xia, Z.L.; Pan, Z.Z. Divergent processes and trends of desertification in Inner Mongolia and Mongolia. *Land Degrad. Dev.* **2020**, *32*, 3684–3697. [[CrossRef](#)]
23. Zhao, L.L.; Jia, K.; Liu, L.; Li, J.; Xia, M. Assessment of land degradation in Inner Mongolia between 2000 and 2020 based on remote sensing data. *Geogr. Sustain.* **2023**, *4*, 100–111. [[CrossRef](#)]
24. Yu, W.Z.; Zhu, M.X.; Shao, L.; Shen, Y.B.; Liu, H.T.; Chen, T.L.; Zhang, H.X.Y. Characteristics of Desertification Change in Lake Basin Area in Gangcha County. *Comput. Mater. Contin.* **2022**, *73*, 3771–3793. [[CrossRef](#)]
25. Bai, Z.F.; Han, L.; Jiang, X.H.; Liu, M.; Li, L.Z.; Liu, H.Q.; Lu, J.X. Spatiotemporal evolution of desertification based on integrated remote sensing indices in Duolun County, Inner Mongolia. *Ecol. Inform.* **2022**, *70*, 101750.
26. Sun, B.L.; Ma, L.; Feng, Q.; Liu, T.X.; Liang, L.T.; Li, H.Y.; Zhou, Y.; Liu, Y. Response of the warming hiatus to changing influences over the Inner Mongolia Autonomous Region. *China Environ. Sci.* **2019**, *39*, 2131–2142.
27. Peng, S.Z.; Ding, Y.X.; Liu, W.Z.; Li, Z. 1 km monthly temperature and precipitation dataset for China from 1901 to 2017. *Earth Syst. Sci. Data* **2019**, *11*, 1931–1946. [[CrossRef](#)]
28. Adam, M.; Hubert, H. Spatial downscaling of European climate data. *Int. J. Climatol.* **2016**, *36*, 1444–1458.
29. Chen, P.F. Monthly NPP Dataset Covering China's Terrestrial Ecosystems at North of 18° N (1985–2015). *J. Glob. Change Data Discov.* **2019**, *3*, 34–41.
30. Yin, H.; Li, Z.G.; Wang, Y.L.; Cai, F. Assessment of Desertification Using Time Series Analysis of Hyper-temporal Vegetation Indicator in Inner Mongolia. *Acta Geogr. Sin.* **2011**, *66*, 653–661.
31. Tu, H.Y.; Jiapaer, G.L.; Yu, T.; Li, X.; Chen, B.J. Analysis of spatio-temporal variation characteristics and influencing factors of net primary productivity in terrestrial ecosystems of China. *Acta Ecol. Sin.* **2023**, *43*, 1219–1233.
32. Lieth, H.; Box, E. Evapotranspiration and primary productivity. *Climatology* **1972**, *25*, 37–46.
33. Shang, S.S.; Lian, L.S.; Ma, T.; Zhang, K.; Han, T. Spatiotemporal Variation of Temperature and Precipitation in Northwest China in Recent 54 Years. *Arid. Zone Res.* **2018**, *35*, 68–76.
34. Man, W.J.; Xu, Y.J. Using NPP and EVI to assess the ecological status of the Sanjiangyuan area. *Grassl. Turf* **2021**, *41*, 1–8.
35. Wang, Z.Y.; Zhong, J.L.; Lan, H.; Wang, Z.B.; Sha, Z.Y. Association analysis between spatiotemporal variation of net primary productivity and its driving factors in Inner Mongolia, China during 1994–2013. *Ecol. Indic.* **2019**, *105*, 355–364. [[CrossRef](#)]
36. Ke, J.; Zhou, D.D.; Hai, C.X.; Yu, Y.H.; Jun, H.; Li, B.Z. Temporal and Spatial Variation of Vegetation in Net Primary Productivity of the Shendong Coal Mining Area, Inner Mongolia Autonomous Region. *Sustainability* **2022**, *14*, 10883. [[CrossRef](#)]
37. Yu, D.S.; Li, H.Y.; Yin, B.L.; Wu, N.T.; Ye, R.H.; Liu, G.X. Spatiotemporal variation of net primary productivity and its response to drought in Inner Mongolian desert steppe. *Glob. Ecol. Conserv.* **2022**, *33*, e01991. [[CrossRef](#)]
38. Zhang, G.G.; Kang, Y.M.; Han, G.D.; Sakurai, K. Effect of climate change over the past half century on the distribution, extent and NPP of ecosystems of Inner Mongolia. *Glob. Change Biol.* **2011**, *17*, 377–389. [[CrossRef](#)]
39. Feng, X.W.; Wu, G.X.; Wang, T.J.; Chai, Z.F. Sandy desertification process and dynamic assessment in Hunshandake sand land. *J. Arid. Land Resour. Environ.* **2020**, *34*, 109–116.
40. Lian, L.; Zhao, X.Y.; Li, X.; Zhang, T.H.; Wang, S.K.; Luo, Y.Q.; Zhu, Y.C.; Feng, J. Detecting sustainability of desertification reversion: Vegetation trend analysis in part of the agro-pastoral transitional zone in inner Mongolia, China. *Sustainability* **2017**, *9*, 211. [[CrossRef](#)]
41. Fan, Z.M.; Li, S.B. Spatio-temporal pattern change of desertification and its driving factors analysis in China-Mongolia-Russia economic corridor. *Acta Ecol. Sin.* **2020**, *40*, 4252–4263.
42. Zhou, Y.G.; Hasi, E.; Wang, Z.R.; Qing, D.; Han, X.J.; Yin, J.; Wu, Z.F. Dynamics of blowouts indicating the process of grassland desertification. *Land Degrad. Dev.* **2022**, *33*, 2885–2897. [[CrossRef](#)]
43. Sivakumar, M.V.K. Interactions between climate and desertification. *Agric. For. Meteorol.* **2007**, *142*, 143–155. [[CrossRef](#)]
44. Jude, N.E.; Patience, C.O. Pattern of household vulnerability to desertification in Yobe state, Nigeria. *GeoJournal* **2022**, *87*, 2699–2717.
45. Moura, M.M.; Walter, L.S.; Lins, T.R.D.S.; Araujo, E.C.G.; da Cunha Neto, E.M.; Santana, G.M.; Brasil, L.D.S.; Silva, T.C. Temporal analysis of desertification vulnerability in Northeast Brazil using Google Earth Engine. *Trans. GIS* **2022**, *26*, 2041–2055. [[CrossRef](#)]
46. Li, X.; Zhang, X.Q.; Xu, X.M. Precipitation and Anthropogenic Activities Jointly Green the China–Mongolia–Russia Economic Corridor. *Remote Sens.* **2022**, *14*, 187. [[CrossRef](#)]

**Disclaimer/Publisher's Note:** The statements, opinions and data contained in all publications are solely those of the individual author(s) and contributor(s) and not of MDPI and/or the editor(s). MDPI and/or the editor(s) disclaim responsibility for any injury to people or property resulting from any ideas, methods, instructions or products referred to in the content.